

Electronic Supplementary Information for

“Characterisation of the temperature-dependent M_1 to R phase transition in W-doped VO_2 nanorod aggregates by Rietveld refinement and theoretical modelling”

Lei Miao,^{a,b*} Ying Peng,^{a,c} Dianhui Wang,^a Jihui Liang,^a Chaohao Hu,^a Eiji Nishibori,^{d,e}

Lixian Sun,^a Craig A. J. Fisher,^f and Sakae Tanemura^{a,f*}

^a Guangxi Key Laboratory of Information Material, Guangxi Collaborative Innovation Center of Structure and Property for New Energy and Materials, School of Materials Science and Engineering, Guilin University of Electronic Technology, Guilin, 541004, P. R. China

^bSchool of Physical Science and Technology, Guangxi University, Nanning 530004, P. R. China

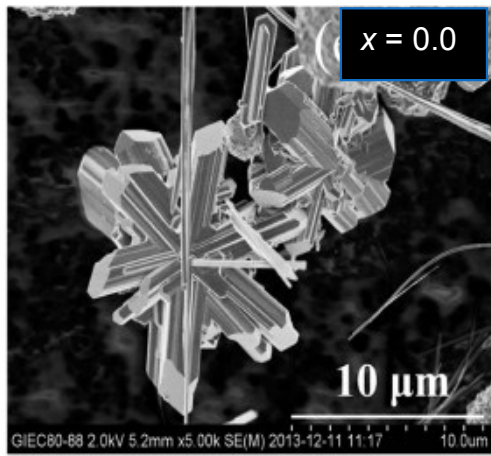
^cDepartment of Materials Physics, Graduate School of Engineering, Nagoya University, Nagoya 464-8603, Japan

^dDivision of Physics, Faculty of Pure and Applied Science, Tsukuba Research Center for Interdisciplinary Materials Science (TIMS), University of Tsukuba, 1-1-1 Tennodai, Tsukuba, Ibaraki 305-8571, Japan

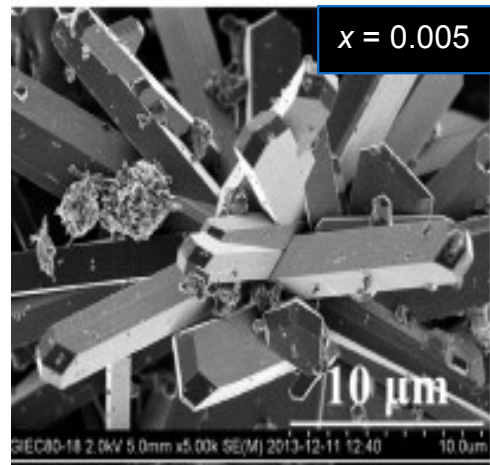
^eStructural Materials Science Laboratory, RIKEN SPring-8 Center, RIKEN, 1-1-1 Koto, Hyogo 679-5148, Japan

^fJapan Fine Ceramics Center, 2-4-1 Mutsuno, Atsuta-ku, Nagoya 456-8587, Japan

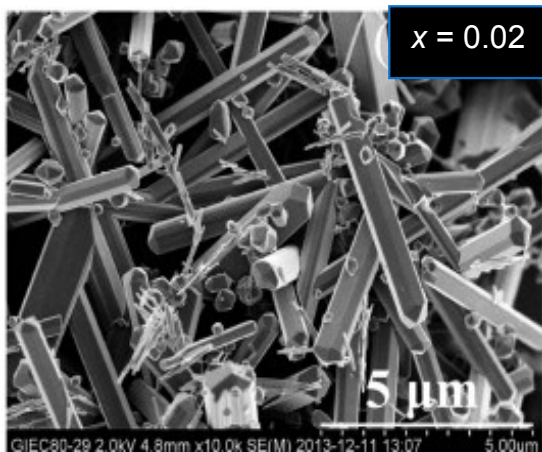
* Corresponding authors. Email addresses: miaolei@guet.edu.cn (L. Miao), fwhy047@nifty.com (S. Tanemura)



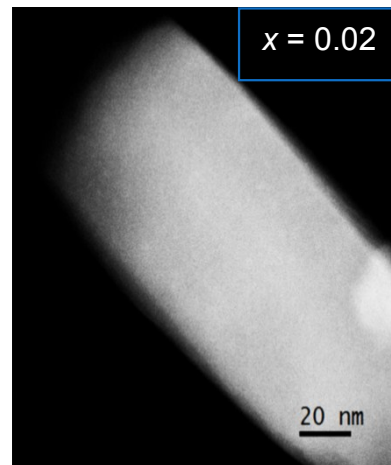
(a)



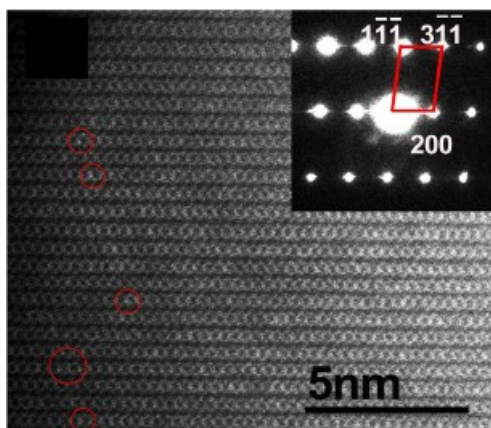
(b)



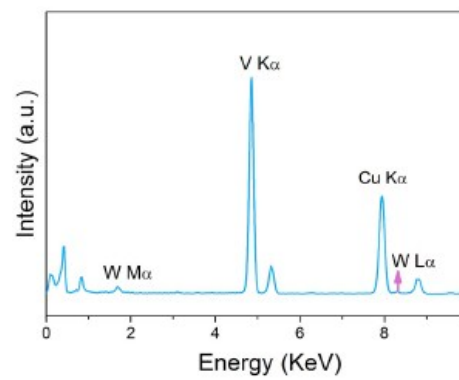
(c)



(d)



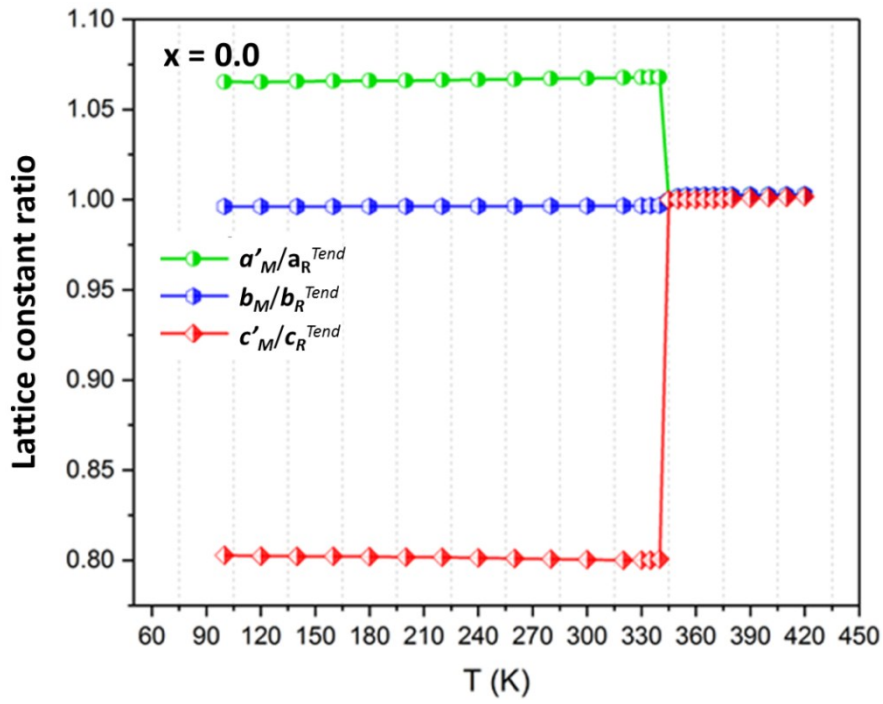
(e)



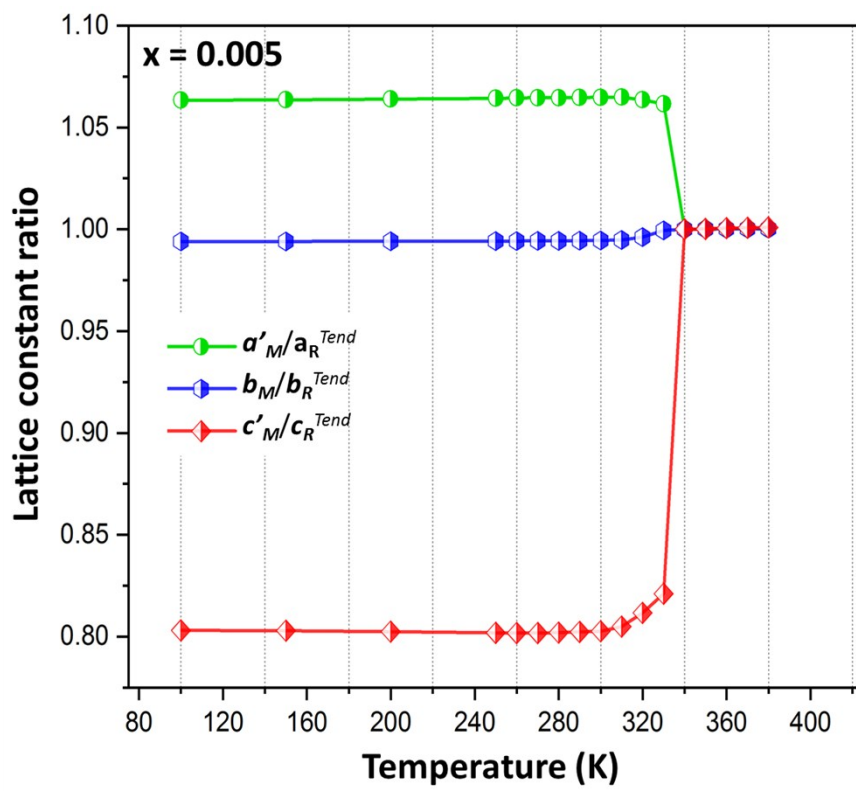
(f)

Fig. S1 (previous page) Low-magnification TEM images of the samples fabricated under the optimised synthesis conditions as explained in the main manuscript: (a) pure VO_2 ; (b) $\text{V}_{0.995}\text{W}_{0.005}\text{O}_2$; and (c) $\text{V}_{0.98}\text{W}_{0.02}\text{O}_2$, and (d) high-magnification TEM image of a nano-rod in (c). The sample was held at a room temperature for those four. (e) HAADF STEM image showing columns of strong contrast corresponding to heavier W atoms (highlighted with red circles) in a nanorod shown as (c). The inset shows the SAED pattern corresponding to the M_1 phase taken down $\langle 011 \rangle$. (f) Energy dispersive spectroscopy spectrum of the region shown in (e) confirming presence of W atoms. The sample was kept at 100 K.

(a)



(b)



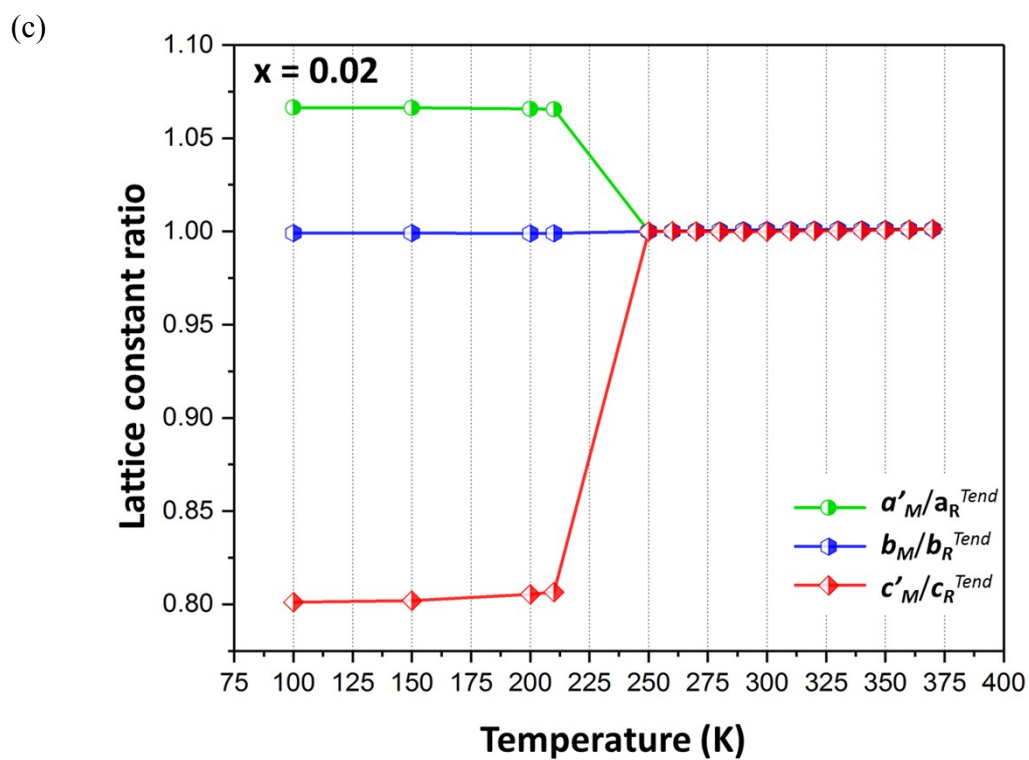
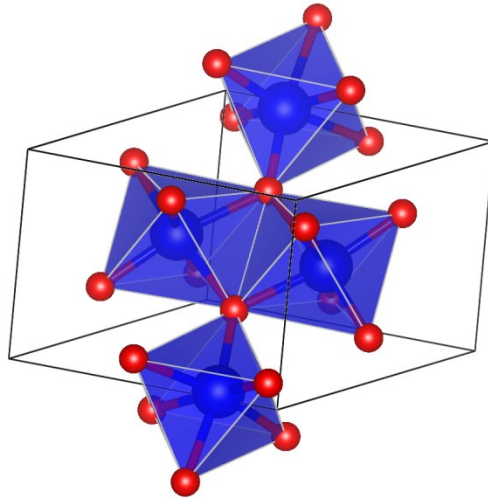


Fig. S2 Lattice constant ratios a'_M/a_R^{Tend} , b'_M/b_R^{Tend} and c'_M/c_R^{Tend} for (a) pure VO₂, (b) V_{0.995}W_{0.005}O₂, and (c) V_{0.98}W_{0.02}O₂.

(a)



(b)

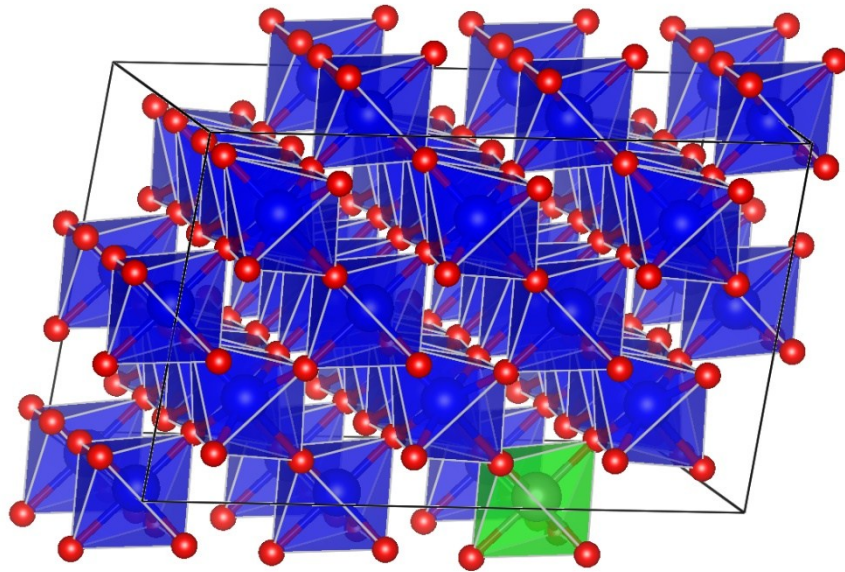


Fig. S3 (a) Crystal structure of M₁-type VO₂ with the unit cell indicated by solid lines, and **(b)** a 2 × 3 × 2 supercell used in calculations of W-doped VO₂. Blue octahedra are centred on V atoms and the green octahedron on the W dopant atom.

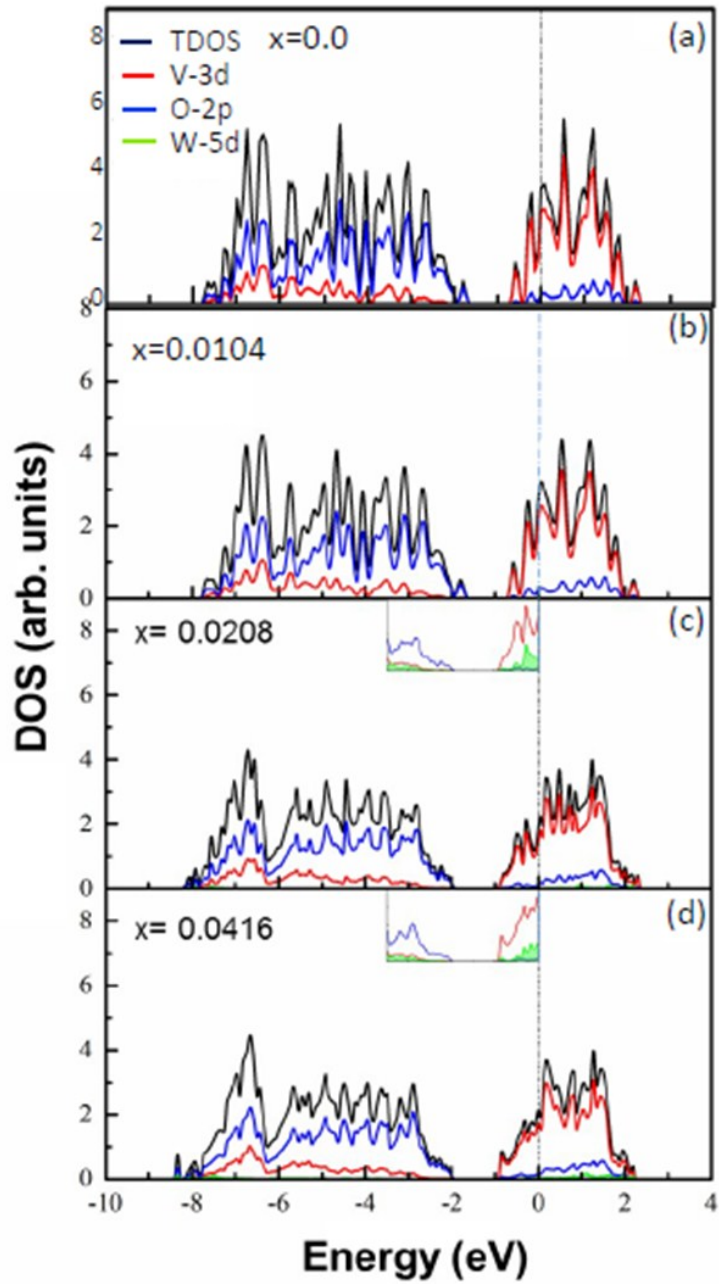


Fig. S4 Calculated partial DOSs of R-type $V_{1-x}W_xO_2$ for **(a)** $x = 0.0$, **(b)** $x = 0.0104$, **(c)** $x = 0.0208$, and **(d)** $x = 0.0416$. DOSs per atom close to the Fermi level are shown as insets in **c** and **d**. The system remains metallic for all W contents examined.

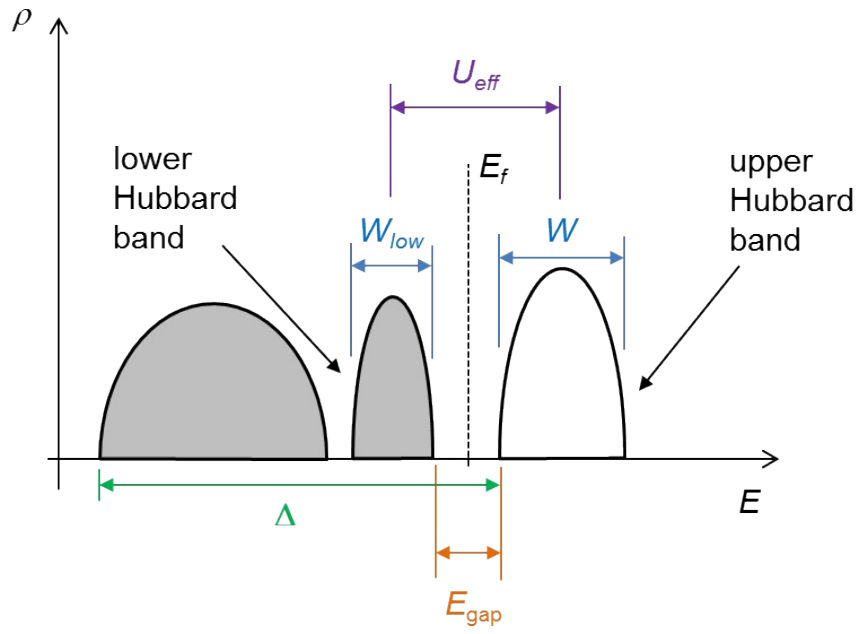


Fig. S5 Schematic diagram of the relation between the various parameters used in the BWC Mott IMT model.

Table S1 Rietveld-refined structure parameters of R-type $V_{0.98}W_{0.02}O_2$ at 380 K in tetragonal space group $P4_2/mnm$ with lattice constants $a = b = 4.56787 \text{ \AA}$, $c = 2.86787 \text{ \AA}$, $\alpha = \beta = \gamma = 90^\circ$.

Site	Coordinates	Occupancy
V1	0.000, 0.000, 0.000	0.98334
W1	0.000, 0.000, 0.000	0.01666
V2	2.284, 2.284, 1.434	0.98334
W2	2.284, 2.284, 2.284	0.01666
O1	1.361, 1.361, 0.000	1.00000
O2	3.207, 3.207, 0.000	1.00000
O3	0.923, 3.645, 1.434	1.00000
O4	3.645, 0.923, 1.434	1.00000

Table S2 Structural parameters for the monoclinic (M_1) and tetragonal (R) phases of undoped and W-doped VO_2 nanorods at different temperatures.

Phase	Parameter	Composition		
		VO_2	$V_{0.995}W_{0.005}O_2$	$V_{0.98}W_{0.02}O_2$
R (tetragonal)	T_{end} (K)	355	340	250
	a_R (Å) (= $a_M = a_M'$)	4.553 ₁	4.556 ₆	4.562 ₂
	b_R (Å) (= $b_M = b_M'$)	4.553 ₁	4.556 ₆	4.562 ₂
	c_R (Å) (= $c_M = c_M'$)	2.851 ₆	2.854 ₂	2.864 ₃
	V_R (Å ³) (= $V_M = V_M'$)	59.11 ₅	59.26 ₁	59.61 ₈
M_1 (monoclinic)	T_{on} (K)	340	280	150
	a_M' (a_M) (Å)	4.851 ₁ (5.756 ₆)	4.851 ₁ (5.754 ₀)	4.864 ₂ (5.759 ₁)
	$a_M' - a_R^{end}$ (Å)	0.298 ₀	0.294 ₄	0.301 ₉
	$\xi_a(T_{on})$ (%)	6.54	6.46	6.62
	b_M' (= b_M) (Å)	4.528 ₂ (4.5282)	4.530 ₈ (4.530 ₈)	4.558 ₂ (4.558 ₂)
	$b_M' - b_R^{end}$ (Å)	-0.024 ₉	-0.025 ₈	-0.004 ₀
	$\xi_b(T_{on})$ (%)	-0.55	-0.57	-0.09
	c_M' (c_M) (Å)	2.284 ₄ (5.383 ₉)	2.288 ₈ (5.383 ₄)	2.296 ₇ (5.379 ₉)
	$c_M' - c_R^{end}$ (Å)	-0.567 ₁	-0.565 ₃	-0.567 ₂
	$\xi_c(T_{on})$ (%)	-19.89	-19.73	-19.80
	V_M' (Å ³)	50.18 ₂	50.30 ₇	50.92 ₂
	V_M'/V_R^{end}	0.8488 ₇	0.8489 ₂	0.8542 ₈
	$T_{-\infty}$ (K)	100	100	100
	a_M' (a_M) (Å)	4.839 ₄ (5.740 ₉)	4.845 ₄ (5.746 ₁)	4.864 ₈ (5.760 ₅)
	$a_M' - a_R^{end}$ (Å)	0.286318	0.288804	0.302588
	$\xi_a(T_{-\infty})$ (%)	6.2883912	6.338077	6.63250
	b_M' (b_M) (Å)	4.525 ₄ (4.525 ₄)	4.532 ₉ (4.532 ₉)	4.558 ₂ (4.558 ₂)
	$b_M' - b_R^{end}$ (Å)	-0.02768	-0.02728	-0.00407
	$\xi_b(T_{-\infty})$ (%)	-0.60793478	-0.59868	-0.0892
	c_M' (c_M) (Å)	2.290 ₅ (5.378 ₈)	2.292 ₀ (5.380 ₆)	2.294 ₃ (5.379 ₃)
$c_M' - c_R^{end}$ (Å)	-0.561085	-0.562244	-0.569559	
$\xi_c(T_{-\infty})$ (%)	-19.6762	-19.6987	-24.8246	
V_M' (V_M) (Å ³)	50.16 ₂ (117.7 ₉)	50.30 ₇ (118.0 ₉)	50.87 ₆ (119.2 ₈)	
V_M'/V_R^{end}	0.8486 ₆	0.8487 ₉	0.8535 ₀	

Note: Values in parentheses are for the monoclinic coordinate system.

Table S3: Volumetric ratios $V_M'/V_R(T_{end})$ and the corresponding volumetric differentials, Ω , for nanorods with three different W dopant levels spanning the corresponding temperature ranges $T_{on} \leq T \leq T_{end}$: (a) pure VO_2 , (b) $\text{V}_{0.995}\text{W}_{0.005}\text{O}_2$, and $\text{V}_{0.98}\text{W}_{0.02}\text{O}_2$.

(a)

VO_2		
T (K)	$V_M'/V_R(T_{end})$	Ω (%)
T_{on} 340	0.848 ₉	-15.1 ₁
T_1 345	0.995 ₅	-0.451 ₅
T_2 350	0.999 ₅	-0.053 ₀
T_{end} 355	1.00	0.00

(b)

$\text{V}_{0.995}\text{W}_{0.005}\text{O}_2$		
T (K)	$V_M'/V_R(T_{end})$	Ω (%)
T_{on} 280	0.848 ₉	-15.1 ₀
T_1 290	0.849 ₄	-15.0 ₆
T_2 300	0.849 ₉	-15.0 ₁
T_3 310	0.852 ₆	-14.7 ₃
T_4 320	0.859 ₉	-14.0 ₁
T_5 330	0.871 ₂	-12.8 ₈
T_{end} 340	1.00	0.00

(c)

$V_{0.98}W_{0.02}O_2$		
T (K)	$V_M'/V_R(T_{end})$	Ω (%)
T_{on} 150	0.854 ₃	-14.5 ₇
T_1 200	0.857 ₃	-14.2 ₆
T_2 210	0.857 ₉	-14.2 ₁
T_{end} 250	1.00	0.00

Table S4: Hubbard-band parameters for V-3*d* orbitals extracted from DOSs of the M₁ phase and used in the BWC-Mott IMT model.

Parameter	Dopant content, x			
	0.0	0.0104	0.0208	0.0416
Upper Hubbard band width, W (eV)	2.345	2.489	2.650	2.828
Band splitting, U_{eff} (eV)	3.349	3.219	3.121	3.023
W/U_{eff}	0.700	0.758	0.849	0.935
Lower Hubbard band width, W_{low} (eV)	0.442	0.452	0.529	0.637
Charge-transfer energy, Δ (eV)	5.66	5.71	5.83	5.99
Band gap, E_{gap} (eV)	0.510	0.382	0.217	0.076

Notes: U_{eff} is the difference between the weighted average energy of the lower Hubbard band and that of the upper Hubbard band; Δ is the gap between the bottom of the O 2*p* band and the bottom of the upper Hubbard band (conduction band minimum).

Table S5 Ratios between $1-W/U_{eff}$ and volumetric differential, Ω , for different W contents, x .

Dopant content, x	T_{on} (K)	W/U_{eff}	$1-W/U_{eff}$	Ω (%)	$(1-W/U_{eff})/\Omega$	$\Omega/(1-W/U_{eff})$
0.0	340	0.700	0.300	-0.1511	-1.9855	-0.2159
0.005	280	0.729	0.271	-0.1510	-1.7947	-0.2073
0.020	150	0.849	0.151	-0.1457	-1.0360	-0.9649

Note: $1-W/U_{eff}$ corresponds to the energy ratio from the apex of the hypothetical phase boundary between insulator and metal state in an f vs W/U_{eff} diagram.

Conventions and notation used in the analysis

(i) Lattice constants

The unit cell of the M_1 phase is monoclinic and can be described using the four lattice constants a_M , b_M , c_M and β (see Fig. S1), which we label collectively as Λ_M . The R phase is tetragonal and can be described using the three lattice constants a_R , b_R and c_R , where $a_R = b_R$, represented collectively by Λ_R . To compare the M_1 and R phases directly, we also calculated orthogonalised lattice parameters for the M_1 phase, as shown in Fig. S1, denoted by a'_M , b'_M and c'_M , and collectively as Λ'_M . a'_M , b'_M , and c'_M are related to a_M , b_M , c_M and β according to $a'_M = a_M \cos(\beta - 90^\circ)$, $b'_M = b_M$ and $c'_M = c_M - a_M \sin(\beta - 90^\circ)$.

(ii) IMT temperatures

We used two different procedures to identify the onset temperature, T_{on} , for the IMT: (a) the temperature at which the R (220) peak first appeared on the shoulder of the M_1 (022) peak in the XRD pattern, and (b) the temperature at which a noticeable change in the gradients of plots of orthogonalised lattice parameters of the M_1 phase on was observed. The endset temperature, T_{end} , was defined as the temperature where $a'_M = b'_M$ ($= a_R = b_R$) and $\beta = 90^\circ$.

The conventional phase change temperature, T_c , was taken as the mean of the onset and endset temperatures of the IMT, i.e., $T_c = (T_{on} + T_{end})/2$. For temperature $T_{-\infty}$ we took the lowest temperature below T_{on} accessible with our equipment, viz., 100 K. This temperature was

sufficiently low for thermal expansion effects on the lattice parameters of the M_1 phase to be ignored.

(iii) Axial ratios

Ratios between the lattice constants in each axial direction of the M_1 phase at a given temperature and the lattice constants of the R phase at T_{end} , $\xi(T)$, were calculated as

$$\xi_i(T) = \frac{\Delta i'_M(T)}{i_R(T_{end})} \equiv \frac{\Delta i'_M(T)}{i'_M(T_{end})}, \quad (\text{Eq. S1})$$

where $i = a, b$ and c , and $\Delta i'_M(T)$ is the difference in (orthogonal) lattice parameter i between the M_1 phase at temperature T and that of the R phase at T_{end} .

(iv) Volumetric differentials

The volumetric differential, Ω , was defined as the difference in unit-cell volumes of the M_1 phase (using an orthogonalised basis) at temperature T , $V'_M(T)$, and the R phase at the endset temperature, $V_R(T_{end})$, divided by $V_R(T_{end})$, i.e.,

$$\Omega(T) = \frac{V'_M(T) - V_R(T_{end})}{V_R(T_{end})} = \frac{V'_M(T)}{V_R(T_{end})} - 1 \quad (\text{Eq. S2})$$

S2)

The unit-cell volume ratio $V'_M(T)/V_R(T_{end})$ can be written as

$$\begin{aligned}
\frac{V_M'(T)}{V_R(T_{end})} &= \frac{\prod_{i=a}^c (i_{M'}(T))}{\prod_{i=a}^c (i_{R}(T_{end}))} = \frac{a_M'(T)b_M'(T)c_M'(T)}{a_R(T_{end})b_R(T_{end})c_R(T_{end})} \\
& \left(\equiv \frac{a_M'(T)b_M'(T)c_M'(T)}{a_R(T_{end})b_R(T_{end})c_R(T_{end})} \right) \\
&= \frac{a_M'(T)}{a_R(T_{end})} \times \frac{b_M'(T)}{b_R(T_{end})} \times \frac{c_M'(T)}{c_R(T_{end})} \\
&= L_a(T)L_b(T)L_c(T) \\
&= \prod_{i=a}^c L_i(T)
\end{aligned} \tag{Eq. S3}$$

where $L_i =$ is the ratio between the orthogonalised lattice constant of the M_1 phase and corresponding lattice constant of the R phase at T_{end} for each crystallographic axis i .

A negative Ω indicates that the M_1 phase is compressed relative to the R phase, whereas a positive Ω indicates that it is expanded.